Quaternary International 380-381 (2015) 382–390

Contents lists available at ScienceDirect

Quaternary International

journal homepage: www.elsevier.com/locate/quaint

Confluent flow impacts of flood extremes in the middle Yellow River

Hongming He [a, *], Yong Q. Tian [b], Xingmin Mu [a, *], Jie Zhou [a], Zhanbin Li [a], Nannan Cheng [a, c], Qingle Zhang [a, c], Soksamnang Keo [a], Chantha Oeurng [d]

[a] State Key Laboratory of Soil Erosion and Dryland Farming on Loess Plateau, Northwest of Agriculture & Forestry University, and Institute of Soil and Water Conservation, Chinese Academy of Sciences & Ministry of Water Resources, Yangling, Shaanxi, 712100, China
[b] Institute for Great Lakes Research, Central Michigan University, Mt. Pleasant, MI, 48859, USA
[c] Graduate University, Chinese Academy of Sciences, Beijing, China
[d] Department of Rural Engineering, Institute of Technology of Cambodia, Russian Federation Blvd, PO. Box 86, Phnom Penh, Cambodia

ARTICLE INFO

Article history:
Available online 5 March 2015

Keywords:
Flood extremes
Flood frequency
Sediment transportation
Artificial intelligence neural network
The middle Yellow River

ABSTRACT

Flood disaster has been one of the most frequent and devastating forms in middle Yellow River, China. Huge flood events transport sediments from upstream to downstream, and lead to changes of river morphology, such as river bed slope, channel roughness, and flood routing process. Flood disasters in the middle Yellow River were constantly caused by backwater effects due to multiple river stream confluence effects. The study aims to investigate confluent flood flow effects on flood routing processes, river morphology, and human activities based on a proposed flood flow model. The proposed model is constructed through coupling hydraulic equations, artificial intelligence neural network and probability theory. Flood frequency analysis is coupled with studies of hydrological routing processes that reduce the flood capacity of the rivers. Flood routing to the confluence were simulated using kinematic wave theory. Case studies have been carried out through field work and model simulation during the past years. Findings are achieved as followings. Firstly, flood frequency at the confluence implies that the confluent extreme flood occurs more frequently in the main streams than that in the tributaries due to influential intensity of East-Asian summer monsoon. Secondly, river morphology was altered partly due to complex flood routing processes in the middle Yellow River under the operation of Sanmenxia Reservoir. The alternated river channels changed the boundary conditions of flood routing, especially for backwater. Bed slopes have greater impacts on flood routing process than roughness does when there is larger flood flow. Finally, the evolution process of the sediment transportation is closely linked with the operations of the Sanmenxia Reservoir.

1. Introduction

Historically, flood extremes caused the most frequent and devastating forms of disasters (Zolina et al., 2004; Herget and Meurs, 2010; Kehew et al., 2010; Diodato and Bellocchi, 2012; Naidu et al., 2012; Tramblay et al., 2012). Flood disasters in the middle Yellow River were constantly caused by backwater effects due to the multiple river stream confluence effects (Qian, 1992; Yu and Lin, 1996; Wang, 2004; He et al., 2006, 2008). Much of the sediment is deposited on the channel bottom when the river flows downstream. Huge flood events transport sediments from upstream to downstream, and lead to changes of river morphology, such as river bed slope, channel roughness (He et al., 2006, 2008). River banks are frequently breached after heavy rains, leading to catastrophic floods which are regularly responsible for heavy loss of life and economic damage in the area (Cunnane, 1988; Burn, 1990, 1997; Bobee et al., 1996; Jain and Lall, 2000; Jun-Haeng et al., 2001; McKillop and Clague, 2007; Greenbaum et al., 2010; Herget and Meurs, 2010; Kehew et al., 2010). The operation of Sanmenxia Reservoir is regarded as a key contributor to severe silting and backwater refluxing (Qian, 1992; Yu and Lin, 1996; Wang, 2004; He et al., 2006, 2008).

The frequency of large-scale flood events shows an increasing trend in the middle Yellow River basin (Qian, 1992; Yu and Lin, 1996; Wang, 2004; McKillop and Clague, 2007). Flood frequency analysis has often been used previously in studying the trend of river floods (Beven, 1997; Macdonald and Werritty, 2001; Glaser and Stangl, 2003). Various indices, including skewness coefficient, Monte Carlo experiments distribution functions of normal, three-

* Corresponding authors.
E-mail addresses: hongming.he@yahoo.com (H. He), xmmu@ms.iswc.ac.cn (X. Mu).

http://dx.doi.org/10.1016/j.quaint.2015.01.048
1040-6182/

parameter lognormal, Gumbel, Pearson Type 3, Weibull, Pareto, and uniform, have been introduced to monitor river floods on the basis of the regional flood characteristics (Cunnane, 1988; Burn, 1990, 1997; Bobee et al., 1996; Jain and Lall, 2000; Jun-Haeng et al., 2001; Javelle et al., 2002; Palmer and Raisanen, 2002; Christensen and Christensen, 2003; Mudelsee et al., 2003; Greenbaum et al., 2010; Herget and Meurs, 2010; Naidu et al., 2012). These flood indices are effective in relating flood dynamics to precipitation. Simple correlation coefficients of flood discharges between rivers have been used to describe the frequency distribution of historic flood series (Obled and Creutin, 1986; Rao and Hsieh, 1991; Hisdal and Tveito, 1993; Loboda et al., 2005; He et al., 2006; Alpert et al., 2008). With gauge data, non-parametric multivariate empirical orthogonal function model is efficient to address the relationship between flood events of rivers (He et al., 2006).

Flood routing computational schemes are mostly derived from the Saint–Venant equations (Daluz, 1983; Cunnane, 1988; Ramamurthy, 1990; Camacho and Lees, 1999; Carrivick, 2006; Elleder, 2010) and other simplified wave models such as the kinematic wave, non-inertia wave, quasi-steady dynamic wave, and gravity wave approximations (Walters et al., 1980; Begin, 1986; Bartholy and Pongrácz, 2007; McKillop and Clague, 2007; Alpert et al., 2008; Elleder, 2010; Greenbaum et al., 2010). The common issues reported in previous studies are that simplified kinematic wave and gravity wave models were unable to account for the downstream backwater effect, and were not suitable for modeling the flood wave propagation in mild-sloped rivers. Special attentions have been paid to the investigation of the distinctive drainage characteristics of the middle Yellow River in the study of flood routing to simulate the flood wave propagation with a downstream backwater effect of complex flood routing, such as bidirectional flow (He et al., 2006, 2008). A bidirectional flood flow evolution computation scheme is developed and efficiently used to simulate the complicated flood flow evolution according to the complex flood flow situation in the middle Yellow River (He et al., 2006, 2008). Computational scheme for bidirectional flow is focused on modeling of backwater flood flows travelling in the opposite directions.

Flood flow and sediment transport in reservoir are important in addressing engineering hydrodynamics research. Conventional methods and models available for estimation of reservoir sedimentation process differ greatly in terms of complexity, inputs, and other requirements (Jain and Lall, 2000; Jun-Haeng et al., 2001; Javelle et al., 2002; Palmer and Raisanen, 2002). Quantitative analysis is required for understanding of the character of the sediment in motion (Ramamurthy, 1990; Camacho and Lees, 1999; Carrivick, 2006). A number of empirical and semi-empirical sediment transport formulae have been developed for use in riverine applications (Obled and Creutin, 1986; Rao and Hsieh, 1991; Hisdal and Tveito, 1993; Carrivick, 2006; McKillop and Clague, 2007; Alpert et al., 2008). However, estimation of reservoir sedimentation has been the subject for quite a long time, and it is not an easy task due to complicated simultaneous processes involved such as sediment transport, erosion, and deposition. In recent years, the artificial neural network ANN technique has shown excellent performance in regression, especially when used for pattern recognition and function estimation (ASCE Task Committee on Application of the Artificial Neural Networks in Hydrology, 2000a, 2000b). It is a highly nonlinear tool that can capture complex interactions among the input and output variables without any prior knowledge about the nature of these interactions. In comparison to conventional, ANNs can tolerate imprecise or incomplete data, approximate information, and presence of outliers and are well suited to this problem (Sudheer et al., 2002; McKillop and Clague, 2007).

The study aims to investigate flood extremes impacts in the middle Yellow River in perspectives of occurrence frequency, refluxing flood routing process, and river morphology changes along with sediment transportation. The characteristics of flood wave propagation under different flood routing boundary conditions is investigated by backwater refluxing computation scheme, followed by analysis of impacts of flood propagation and sediment transportation on river morphology. The simulation analysis is able to improve our understanding of flood routing of backwater refluxing and sediment transportation in the middle Yellow River.

2. Study area

Our study area is in the middle of Yellow River (between Hekou to Huanyuankou–Taohuayu) spanning from (35° N, 105° E) to (41° N, 115° E) as displayed in Fig. 1. The site has a drainage area of 32,354 km^2, which accounts for 43% of the whole Yellow River watershed. We focus on the main stream and its two tributaries, the Weihe River and the Luohe River. The Luohe River is the tributary of the Weihe River which flows into the middle Yellow River at Tongguan. The elevation of Tongguan controls the base level of the Weihe River, and influences the operation behaviours of Sanmenxia Reservoir (construction in1957–1960 and reconstruction in 1969–1978). The confluence area of the middle Yellow River network consists of the main river stream and its four tributaries, including Weihe River, Jinghe River, Luohe River and Fenhe River in the middle Yellow River.

Annual precipitation in the study area ranges from 300 mm to 1000 mm. About 48% of the annual totals (145 mm–480 mm) fall in the summer season (from July to August) in the form of rainstorms (rainfall amounts are over 50 mm in 24 h). Floods occur frequently after rainstorms. They transport large amount of sediments along the Weihe River and the middle Yellow River and finally deposits them in the lower Weihe River. The fluvial sediments gradually change river channel conditions, such as river bed elevation and roughness. Improper human activity, such as the construction of Sanmenxia Dam, also contributed to the shrinkage of river channels in the study area. Consequently, backwater happened in the middle Yellow River basin due to hydraulic condition changes.

3. Material and methods

3.1. Data collection

A catalogue of historic flood events for the study area is compiled primarily from the archives of Systematic Research and Countermeasures for Huge Natural Disasters (China Disaster Prevention Committee, 1993), and using documents on China History Floods before 1990 (Huang, 1989). Gauge data (1950–2010) collected from the State Flood Control and Drought Relief Headquarters is used to improve the accuracy of the flood evaluation in the study area. Gauge data of 17 flood events were collected in different time periods from 1954 to 2010, of which four flood events were used to calibrate the model, and four others were selected to examine the model efficiency through simulation results. Input data to simulation model include topographic, hydraulic and hydrometric datasets. Topographic data, such as river channel roughness, river bed slope, distance between particular cross-sections, were extracted from 30-m Digital Elevation Model (DEM, from IRSA, CAS). Hydraulic and hydrometric data such as flood flow radius, width, and cross-section area, flood flow velocity, discharge and water level in each cross-section were obtained from gauge data compiled in the State Flood Control and Drought Relief Headquarters (State Flood Control and Drought Relief Headquarters, 1992).

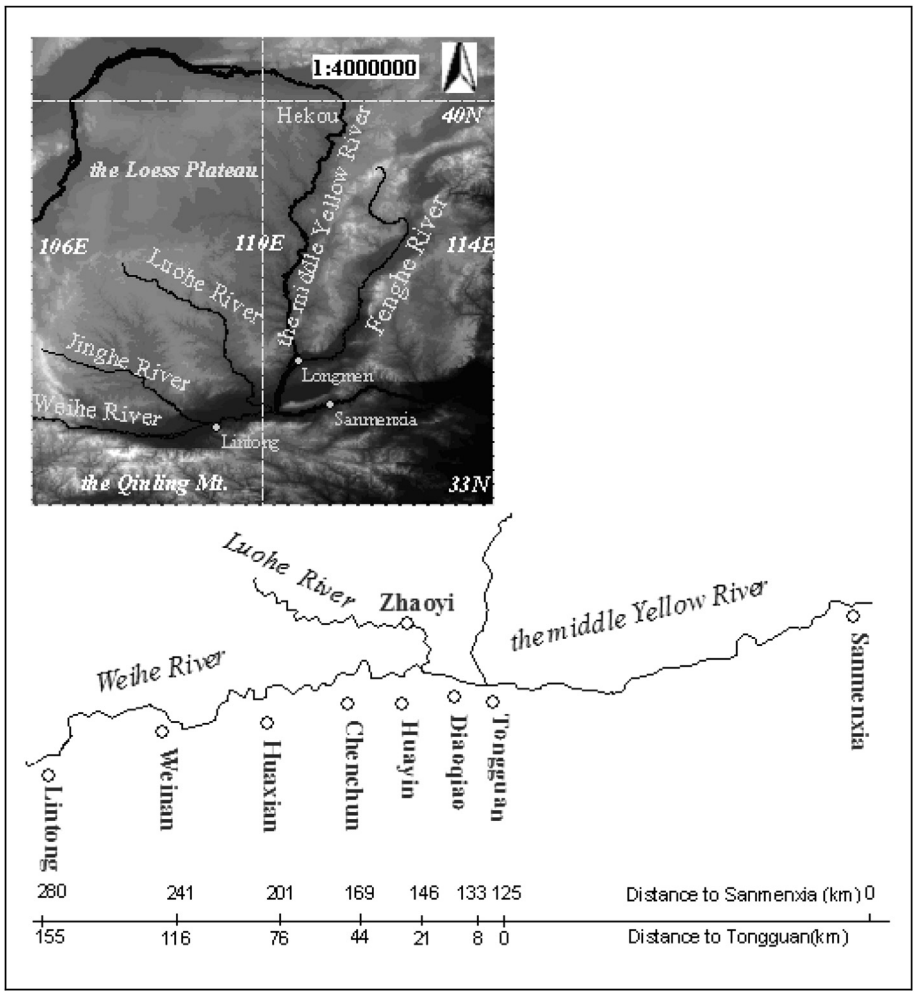

Fig. 1. Sketch map of study area in the middle Yellow River.

3.2. Probability analysis of flood extremes by correlation coefficient matrix

The frequency of large-scale flood events shows an increasing trend in the middle Yellow River basin. Flood frequency occurrence is analyzed through non-parametric, multivariate, empirical, orthogonal function matrix model.

With gauge data, a non-parametric multivariate empirical orthogonal function model is used to address the relationship between flood events of rivers (He et al., 2006). The model defines the flood time coefficient matrix (Θ) as the product of a spatial matrix and a temporal matrix. The spatial matrix (X) represents the relationship between peak flood discharges or water levels at different sites. The temporal matrix (F) represents the relationship between individual discharges or water levels in a flood series. If we use matrix Θ to represent the time coefficient of discharge Q at different stations and a series of flood events, then it can be computed by equation (1) as below.

$$\Theta = X'F \tag{1}$$

The above equation represents interactive behaviors of flood discharge Q between spatial and temporal patterns. The two matrix variables X and F can be expressed as:

$$X = \begin{bmatrix} X_1 \\ X_2 \\ X_3 \end{bmatrix} \tag{2}$$

where X_i is the eigenvector of the correlation coefficient matrix of flood discharge between gauge stations (i, $1 \le i \le 3$).

$$F = \begin{bmatrix} q_{1,1} & q_{1,2} & q_{1,3} & \cdots & q_{1,m} \\ q_{2,1} & q_{2,2} & q_{2,3} & \cdots & q_{2,m} \\ q_{3,1} & q_{3,2} & q_{3,3} & \cdots & q_{3,m} \end{bmatrix} \tag{3}$$

where q_{ij} is the normalized discharge at station i in the flood event j ($1 \le j \le m$). From equations (1)–(3), we get the time coefficient matrix (Θ) of flood discharge Q in station i

$$\Theta = [X_1 \quad X_2 \quad X_3] \cdot \begin{bmatrix} q_{1,1} & q_{1,2} & q_{1,3} & \cdots & q_{1,m} \\ q_{2,1} & q_{2,2} & q_{2,3} & \cdots & q_{2,m} \\ q_{3,1} & q_{3,2} & q_{3,3} & \cdots & q_{3,m} \end{bmatrix} \tag{4}$$

A higher absolute value of time coefficient (Θ) indicates a higher probability of confluence flood occurrence. By using the time correlation coefficient of flood discharges, this non-parametric multivariate empirical orthogonal function model improves

preciseness of frequency analysis in the temporal and the spatial dimension (He et al., 2006).

3.3. Bidirectional flow model for backwater refluxing

Boundary condition is one of the key factors in computation of hydrological modeling. We introduced bidirectional flood flow evolution computation schemes to simulate the complicated flood flow evolution according to the complex flood flow situation in the middle Yellow river (He et al., 2006, 2008). Based on Saint Venant equation, the flow routing process and sediment transportation of backwater evolution in flood event is viewed as one dimensional unsteady flow described through St. Venant equation based on equations of continuity and momentum as Functions (5–6).

For flood flow routing,

$$\begin{cases} \dfrac{\partial Q}{\partial x} + B\dfrac{\partial Z}{\partial t} = q_L \\ \dfrac{\partial Q}{\partial t} + 2v\dfrac{\partial Q}{\partial x} + \left(gA - BV^2\right)\dfrac{\partial Z}{\partial x} - V^2\dfrac{\partial A}{\partial x}\Big|_z + g\dfrac{n_m Q|Q|}{AR_h^{4/3}} = 0 \end{cases} \tag{5}$$

For sediment transportation,

$$\begin{cases} \dfrac{\partial Q_s}{\partial x} + (1-P)\dfrac{\partial Z}{\partial t} = q_s \\ \dfrac{\partial Q_s}{\partial t} + 2v\dfrac{\partial Q_s}{\partial x} + \left[gA - (1-P)V^2\right]\dfrac{\partial Z}{\partial x} - V^2\dfrac{\partial A_s}{\partial x}\Big|_z + g\dfrac{n_m Q_s \partial_s |Q_s|}{A_s R_h^{4/3}} = 0 \end{cases} \tag{6}$$

where Q is flood discharge (m^3/s), Q_s is sediment discharge (m^3/s), x is the coordinate horizontal in flow direction, B is the velocity of propagation of the kinematic wave (m/s), P is porosity of the bed deposit (volume of voids divided by the total volume of sample), Z is water level (m), q_L is the lateral inflow per unit time per unit channel length (m^2/s), q_s is the lateral sediment inflow per unit time per unit channel length (m^2/s), t is the time (s), V is flood flow velocity (m/s);g is acceleration due to gravity (m/s^2), A is cross-sectional area of the flow (m^2); R_h is the hydraulic radius (m), n_m is Manning roughness coefficient. The friction slope S_f is approximated by Manning's equation (Keskin and Agiralioglu, 1997; Ren and Cheng, 2003).

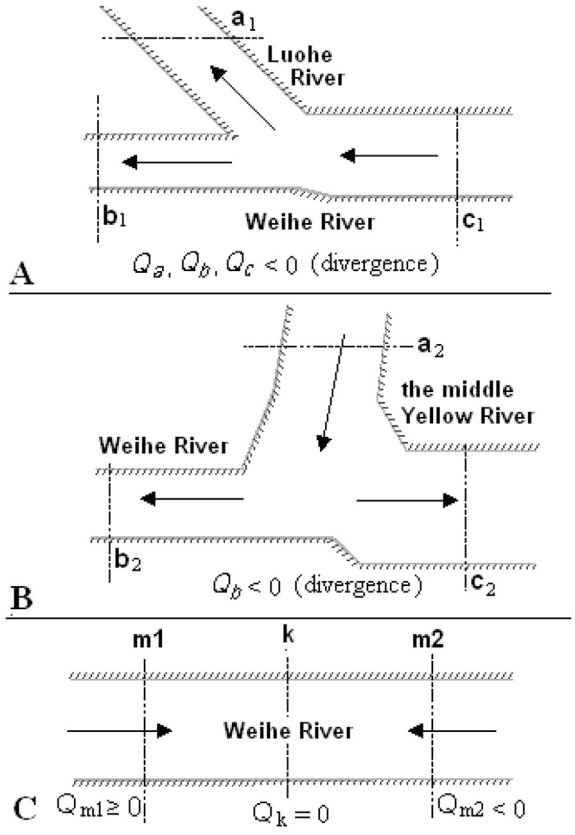

Fig. 2. Computational schemes of backwater refluxing in the middle Yellow River.

We use Preissmann three-point implicit scheme (He et al., 2006, 2008) to solve the channel flow equations and avoid the disturbing effect of the numerical diffusion on the results of modeling. The flow domain is divided into a number of flow reaches. Accordingly, for a point like 'p' located in a rectangular grid, the average values and derivatives are given by,

$$\begin{cases} \dfrac{\partial f}{\partial x} \approx \dfrac{\theta\left(f_{i+1}^{j+1} - f_i^{j+1}\right) + (1-\theta)\left(f_{i+1}^{j} - f_i^{j}\right)}{\Delta x_i} \\ \dfrac{\partial f}{\partial x} \approx \dfrac{f_{i+1}^{j+1} + f_i^{j+1} - f_{i+1}^{j}}{2\Delta t} \end{cases} \tag{7}$$

where f is the function of Q, Z, A, V. The subscript of f is the identity of different river reaches; the superscript of f depicts different time periods. θ is the time-weighting coefficient. Δx_i is the length of the ith reach in a river. On substituting the average values in Equation (1) for the appropriate items in Equation (7), the following equations are obtained:

$$\begin{cases} -Q_{i-1}^{j+1} + Q_i^j + C_i Z_{i-1}^j + G_i Z_i^{j+1} = D_i \\ E_i Q_{i-1}^{j+1} + G_i Q_i^{j+1} - F_i Z_{i-1}^{j+1} + F_i Z_i^{j+1} = \varphi_i \end{cases} \tag{8}$$

where, Q_1^{n+1} and Z_N^{n+1} are flood discharge and water level at nth time step, Q_1 and Z_N are initial flood flow discharge and water level, t_{n+1} is time step at $n+1$. F_{i+1}, G_{i+1} are approaching coefficients, and initial values are defined as $F_1 = 0$, $G_1 = Q_1 \cdot t_{n+1}$. By using these approaching function and boundaries

$$C_i = \frac{\Delta x_i B_{ij-1/2}}{2\theta\Delta t}$$

$$D_i = \frac{1-\theta}{\theta}\left(Q_{i-1}^j - Q_i^j\right) + C_i\left(Z_{i-1}^j + Z_i^j\right)$$

$$E_i = \frac{\Delta x_i}{2\theta\Delta t} - 2V_{i-1/2}^j + \frac{g}{2\theta}\left(\frac{n^2}{R^{1.33}}\right)_i^j \left|V_{i-1}^j\right| \Delta x_i$$

$$F_i = \left(gA - BV^2\right)_{i-1/2}^j$$

$$\varphi_i = \frac{\Delta x_i}{2\theta\Delta t}\left(Q_{i-1}^j + Q_i^j\right) + \frac{2(1-\theta)}{\theta}V_{i-1/2}^j\left(Q_{i-1}^j + Q_i^j\right) + \frac{1-\theta}{\theta}\left(gA - BV^2\right)_{i-1/2}^j\left(Z_{i-1}^j + Z_i^j\right) + \frac{\Delta x_i}{\theta}\left(V^2\frac{\partial A}{\partial x}\Big|_z\right)_{i-1/2}^j \tag{9}$$

The approaching method was used to estimate flood influence on kinematic wave propagation based on the upper boundary conditions of flood discharge.

The improved boundary scheme for bidirectional flow was focused on modelling of two flood flows of similar magnitudes travelling in the opposite directions. Other cases of bidirectional flows of different magnitudes have been considered in the improved boundary scheme for convergent and divergent flows.

Bidirectional flood flows occur when backwater flows back from the middle Yellow River to the Weihe River (Fig. 2). When two flood flows in opposite directions meet together, a zero flood discharge will occur. Therefore, we can define that,

$$\begin{cases} Q_{m1}^{n+1} = Q_{m2}^{n+1} = 0 \\ Q_{sm1}^{n+1} = Q_{sm2}^{n+1} = 0 \\ Z_{m1}^{n+1} = Z_{m2}^{n+1} \end{cases} \quad (10)$$

and approaching coefficients in Equation (8) can be calculated from Equation (10). However, the confluence cross-section of the two bidirectional flows is relatively difficult to locate as it relates with the state of ebb-and-flow of the two flood flows, and varies with time. Therefore, we use explicit difference solution to solve the problem, and to calculate flood flow parameters at time step of $n\Delta t$.

The computation time interval (Δt) is one of the key parameters in model simulation. Two factors are important in choosing time step in the computation. First, the interval should be short enough to accurately describe the rise and fall of the hydrographs being routed. Second, computation interval should be adjusted by variations of hydraulic features, such as boundary conditions. By considering the propagation of peak flood discharge and water level, we define time interval (Δt) and distance interval (Δx) by the functions described as below.

$$\begin{cases} \Delta t = 0.5 \quad t \le \tau - 0.5 \\ \Delta t = t_p/20 \quad \tau - 0.5 \le t \le \tau + 2\tau \\ \Delta t = T_p/20 \quad t \ge \tau + 2t_p \\ \Delta x = c_f \cdot \Delta t \end{cases} \quad (11)$$

where Δt is time interval (hour), t_p is the time of first occurrence of peak discharge (hour), T_p is the time of peak discharge occurrence in selected cross-section (hour), τ is the time of peak discharge occurrence in the outlet (hour), C_f is the celerity of flood wave propagation (m/s), Δt is distance interval (m). The time intervals range from 0.5 to 1 h. The distance intervals range from 3.1 to 5.5 km for 13 reaches. The ratios of time interval and distance interval ($\Delta t/\Delta x$) are between 3.5 and 6.3.

3.4. Simulation of sediment transportation – artificial neural network model

Sediment scouring and silting is simulated by introducing Multiple Layer Perceptron Artificial Neural Network model (MLP ANN) (Fig. 3). The number of input parameters in the ANN is determined on basis of parameters causing and affecting the underlying process which are also easily measurable at the reservoir site. The number of hidden layers and the number of nodes in each hidden layer are also determined by a trial-and-error procedure. The number of nodes in the hidden layer plays a significant role in ANN model performance. The Sigmoid and Hyperbolic Tangent (*tan h*) transfer functions corresponding to a single (*Sv*) output were used to select the best ANN architecture. In the MLP ANN, connections exist between nodes of different layers, while no such connections exist between nodes within the same layer. The inputs are presented to a network at the input layer, and are acted upon by transformations to produce an output (Haykin, 1999).

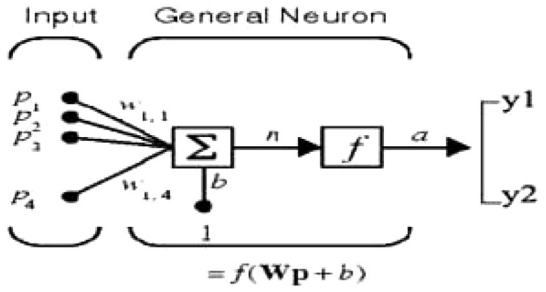

Fig. 3. Computational schemes of backwater model for sediment transportation (Multilayer Neural Network Architecture, P_1 is input water discharge, P_2 is sand discharge, P_3 is input mean water level, P_4 is reservoir water capacity, Y_1 is output sediment between upper/lower reaches, Y_2 is river bed elevation between upper/lower reaches, W is scalar weight of input, f is transfer function).

Suppose that, *P1* is input water discharge, *P2* is sand discharge, *P3* is input mean water level, *P4* is reservoir water capacity, *Y1* is output sediment between upper/lower reaches, *Y2* is river bed elevation between upper/lower reaches, *W* is scalar weight of input, *f* is transfer function which is defined by ΔCf and ΔCnf ($\Delta C_f = f(Q_{fh}, S_f, Q_{fs}, Z_f, V_{fs0}, d_{fs}, J_f, P_f)$, $\Delta C_{nf} = f(Q_{nfh}, S_{nf}, Q_{nfs}, Z_{nf}, V_{nfs0})$), *b* is scalar bias. The neural network learns by adjusting the weights and biases of such connections. In MLP ANN model, flood flow refluxing effects in the Sanmenxia Reservoir of scouring and silting sediment is simulated by transfer Functions (12)

$$\begin{cases} f = \left(\Delta C_f, \Delta C_{nf}\right) \\ \Delta C_{scour} = f(Q_{hscour}, Q_{sscour}, S_{scour}, Z_{scour}, V_{s0scour}, d_{sscour}, J_{scour}, P_{scour}) \\ \Delta C_{silt} = f(Q_{hsilt}, Q_{ssilt}, S_{silt}, Z_{silt}, V_{s0silt}) \end{cases} \quad (12)$$

where, ΔC_{scour} is scouring sediment amount in flood, ΔC_{silt} is silting sediment amount in non-flood, Q_{hscour} is mean water discharge in flood, Q_{hsilt} is mean water discharge in non-flood, Q_{sscour} is ratio of sediment input to Reservoir in flood, Q_{ssilt} is ratio of sediment input to Reservoir in non-flood, S_{scour} is mean sediment inputs in flood, S_{silt} is mean sediment inputs in non-flood, Z_{scourf}, is river water level of downstream in flood, Z_{scourf}, is river water level of downstream non-flood, $V_{s0scour}$ is initial sediment amount of Reservoir in flood, $V_{s0scour}$ is initial sediment amount of Reservoir in non-flood, d_{sscour} *is particle* diameter of input sediment in flood, J_{scour} is river water level slope from upperstream to downstream, P_{scour} is rainstorm distribution in flood area.

4. Results

4.1. Flood frequency analysis from correlation coefficient matrix model

Our modeling results successfully estimated the three huge flood events from 1950 to 2010. Integrated analysis of temporal and spatial characteristics of flood frequency was based on the non-parameters empirical function model (Fig. 4).

The simulation results using the non-parameter empirical function model with time coefficients reveal the relationship between flood probability and the true intensity of floods at the confluence. Computed time coefficient of confluent flooding probability for July (marked as Θ_7) matched the discharges in real flood events very well. The model performance is consistent with other flooding years. Similarly, the low Θ_7 value stands for the low probability of floods at the confluence. For example, in the event of July, 1971, the Θ_7 value was 0.53, and the normalized values of the flood discharge for the same three stations were −0.78, −0.49 and 2.48. The corresponding gauged discharges were 1280 m^3/s, 206 m^3/s, and 14,300 m^3/s. Based on our time coefficient model, we predicted flood events from 1996 to 2010. In July, 2001, the Θ_7 value was 1.45, and the normalized values of flood discharge were 1.03, 0.45, and 1.52. In this scenario, a small flood event occurred at the confluence of the middle Yellow River, Weihe River and Jinghe River. In the events of August 26th, 27th and 31st, 2003, the

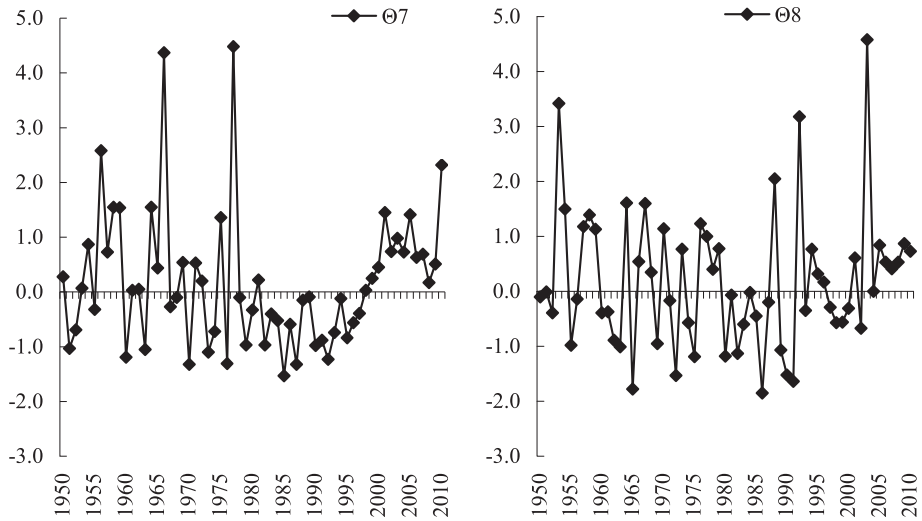

Fig. 4. Computed time coefficients of confluent flooding from correlation coefficient matrix model probability (Θ_7 in July and Θ_8 in August).

discharges reached 1140 m^3/s, 5100 m^3/s and 7230 m^3/s. Computed time coefficient of confluent flooding probability in August (marked as Θ_8) was 4.58, and the normalized values of the flood discharges were 2.65, 3.75 and 3.24. In this scenario, there was a huge flood at the confluence of the middle Yellow River, Luohe River, Jinghe River and Weihe River.

Model results identified that the correlation coefficients of flood discharges between different stations are capable of describing the spatial distribution characteristics of flood frequency at the confluence. The spatial characteristics of flood frequency derived from the correlation coefficient analysis and R-squared values of the regression model (the methods of analyzing the relationship of flood discharges between stations) were compared to the documented historic flood events. Coefficient of variation (CV, ranging from 0 to 1) represents the variation degree of water-related variables in hydrology. The greater CV value means the higher probability of variation. The CV values of the annual flood discharges varied from 0.36 to 0.52 (Yellow River and Weihe River) to 0.87–0.94 (Jinghe River and Luohe River) (Table 1). Since the Fenhe River and Weihe River are tributaries of the middle Yellow River, and Jinhe and Luohe are tributaries of Weihe River, the values imply that the variation of the annual flood discharges is lower in the main streams than that in the tributaries. This can be explained by the influence of the summer monsoon. In an earlier rainy season, flooding may occur in the tributary several days before in the main stream, so that the effect of the tributary flood flow on the main stream is insignificant.

Table 1
Coefficient of variation (*CV*) values in the middle Yellow River Basin.

River name	Coefficient of variation of annual flood discharge
Main stream of Yellow River	0.36
Weihe River.	0.52
Fenhe River	0.63
Jinghe River	0.87
Luohe River	0.94

4.2. Flood refluxing simulation from bidirectional flow model

The numerical model is further applied in investigation of the confluent channels of backwater effects. The results of simulating bidirectional flow in which two floods of similar magnitudes converge in the opposite directions were examined using data from historic flood records including bilateral flow of the Weihe River on June 6, 1992; bilateral flow of Weihe River-Luohe River on Aug 28, 1977; bilateral flow of Weihe River-the middle Yellow River on Aug 25, 2003. Representative of backwater occurrence from bidirectional flow are presented in Fig. 5.

Backwater effects propagate upstream so that the effect of a disturbance is felt upstream as well as downstream. The observed flood discharge and sediment transport and simulated results in Tongguan were determined for a supercritical flow event. Generally, the hydrograph distributions of flood discharge and sediment transport are similar. However, a discrepancy exists in connection with durations and peak values. The occurrences of peak flood discharge and sediment transport are different. There are always time lags of sediment transports behind flood discharge, which varies from 1.8 to 4.3 h. Time lags became greater from the earlier stage in 1970's to 2000's. The magnitude of the backwater resulting from bidirectional flow is relatively small compared with that which occurs when flood flow diverts from the main stream to the tributary. The rising limbs and the recession limbs fluctuated can be regarded as a coupling effect of backwater resulting from bidirectional flow. Through investigation of those historical flood events in the middle Yellow River (1977, 1992 and 2003), the model identified that the shape of flood hydrographs changed with time from high and thin to low and wide (Fig. 5). These changes were accompanied by a delayed occurrence and extended duration of peak flow of progressively later floods. These trends were intensified from the early 1980s. For example, flood hydrographs at Tongguan gauge demonstrate that peak discharges, water levels, flood durations, and backwater conditions changed considerably between 1977 and 2003. Flood hydrographs at the Tongguan gauge show that the peak discharge of the 2003 flood (5200 m^3/s) amounted to only one half of that in 1977 (11,300 m^3/s) but flood duration (with threshold discharge being 950 m^3/s) extended 43 h from 1977 to 2003. The backwater traced back for 17.5 km, and peak discharge of the backwater increased by 42 m^3/s from 1977 to 2003. From the above information, it is evident that flood flow propagation in the middle Yellow River experienced a significant change during the study period. Backwater effects propagate upstream, and disturbance effect is observed upstream and downstream, and water level is likely to increase upstream and decrease downstream.

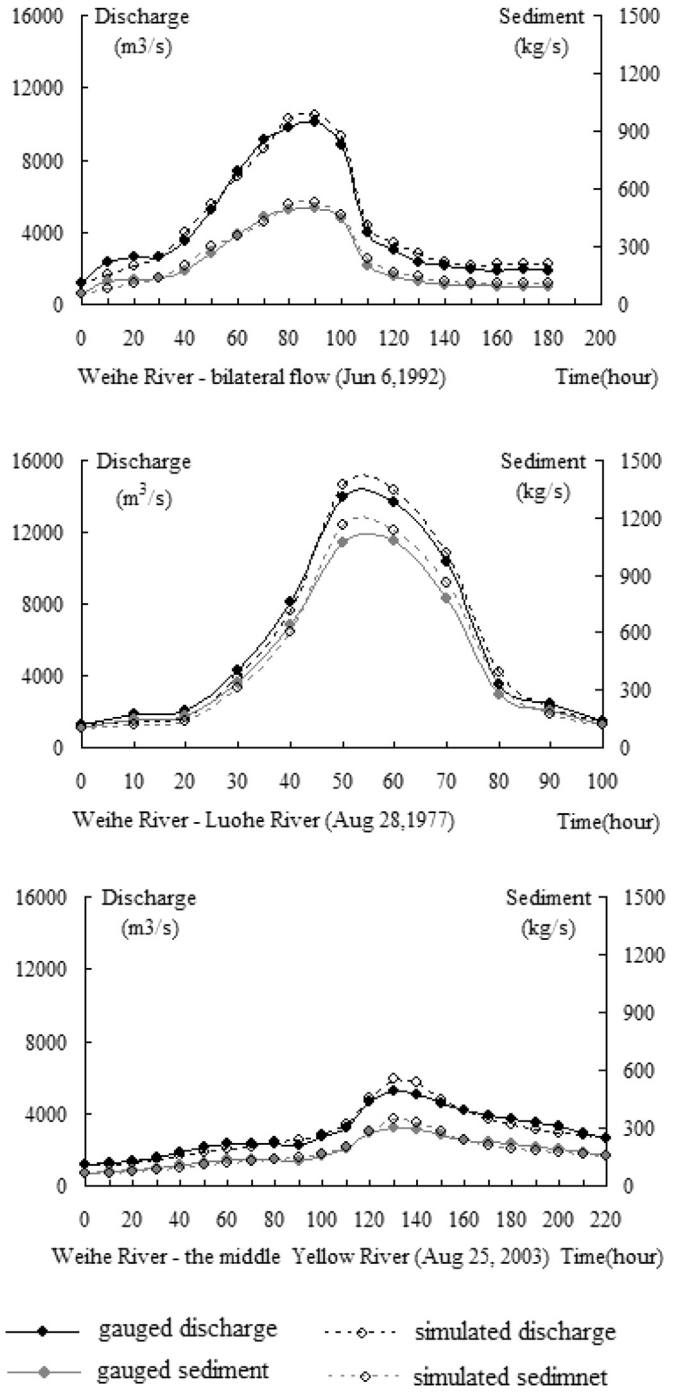

Fig. 5. Simulation of backwater refluxing flow and sediment transport in Tonguan.

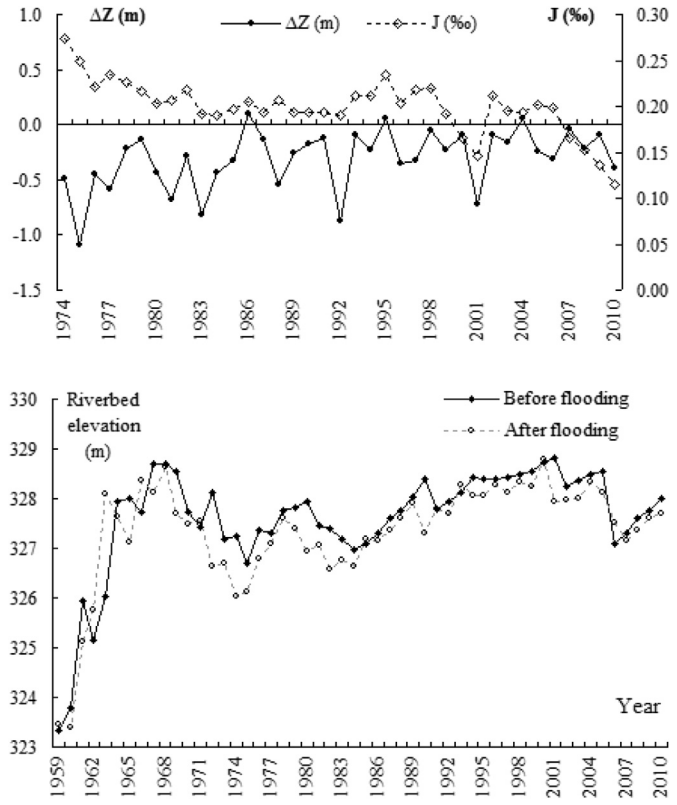

Fig. 6. Flooding impacts on riverbed elevation at Tongguan (1959–2010) (Before flooding, normal flow state before rainstorm-flooding; After flooding, post flow state after rainstorm-flooding).

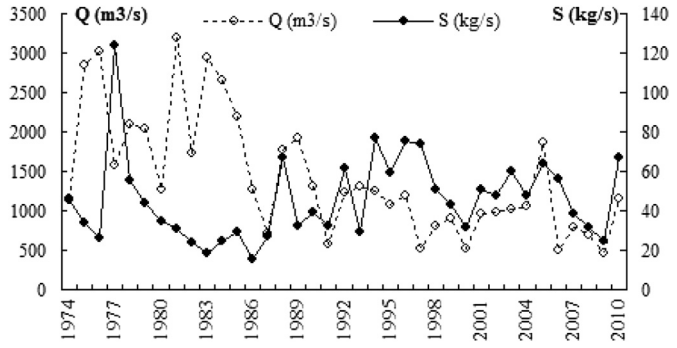

Fig. 7. Simulated flood discharge and sediment transport in Tongguan from MLP ANN model (Q, flood discharge; S, sediment transport; ΔZ, change of river bed elevation between fore-and-aft Sanmenxia Reservoir; ΔJ, change of river slope between fore-and-aft Sanmenxia Reservoir, 1974–2010).

4.3. Sediment transportation of scouring and silting process

The evolution process of the sediment transportation is closely linked with operations of the Sanmenxia Reservoir after it was constructed. The pressure–response relationship between Sanmenxia Reservoir and sediment transportation of scouring and silting process in lower Weihe River was investigated using the Multiple Layer Perceptron Artificial Neural Network model (MLP ANN) model. Simulated results are described in Figs. 6–7.

The river bed was characterized by slight silting, while the sand input and output was in balance before the Sanmenxia Reservoir was built. The reservoir and the river bed of the Weihe River lower reach have been severely silted and the backwater opposites extended rapidly towards the upper stream after construction. However, the amount varied in different periods by some controlled measures. Sediment transportation capacity of the flood flow increased from 52 kg/m^3 in 1962 to 78 kg/m^3 in 2010), and more than 2.12 × 1010 m^3 of sediment was deposited in the lower Weihe River between 1962 and 2010.

When flood flow refluxed, the water level of Tonguan rose quickly followed by the raised water level of Huayin while the discharge-time process was similar, but with relative time lag. Riverbed elevations at Tongguan were mainly controlled by the

water level of Sanmenxia Reservoir, and high water-level duration and water-sand capacity conditions were also contributors.

Changes of peak flood discharge results in fluctuation of the riverbed slope. Lower sediment transport capacity coincides with smaller flood discharge in most periods through the study periods (1974–2010). However, small flood discharge also brought relatively high sediment loads in 1990's. The obvious consequence of the construction of Sanmenxia Reservoir is an elevated riverbed. The riverbed was elevated by almost 5.0 m, from 323.3 in 1959 to 328.3 in 2007. Clearly, sediments transportation alters the river morphologies through elevated river levees and narrowed river channels which were caused by the transported sediments from upstream to the downstream in the middle Yellow River.

5. Conclusions and discussion

Extreme flood disasters in the middle Yellow River that caused by backwater effects is greatly affected by integrated confluence effects of the multiple river streams. Huge flood events transport sediments from upstream to downstream, and lead to changes of river morphology, such as river bed slope, and elevated riverbed. The operation of the Sanmenxia Reservoir is regarded as a key contributor to severe silting and backwater refluxing.

The frequency of large-scale flood events shows an increasing trend in the middle Yellow River basin. Flood frequencies vary with larger floods occurring on a longer cycle according to flood intensities at the confluence area in the middle Yellow River. The correlation coefficients of flood discharges between different stations are capable of describing the spatial distribution characteristics of flood frequency at the confluence. Flood frequency at the confluence implies that the confluent extreme flood occurs more frequently in the main streams than that in the tributaries due to influential intensity of East-Asian summer monsoon.

Complex flood routing processes in the middle Yellow River were altered under changes of river boundary conditions, especially for backwater. A magnitude of the backwater resulting from bidirectional flow is relatively small compared with that which occurs when flood flow diverts from the main stream to the tributary. The rising limbs and the recession limbs fluctuated can be regarded as coupling effect of backwater resulted from bidirectional flow.

The model simulation confirmed that human activities such as constructions of the Sanmenxia Dam, have significant effects on flood characteristics and river morphology. The evolution process of the sediment transportation is closely linked with operations of the Sanmenxia Reservoir.

The need of model improvement is in parameters calibration to deal with the uncertainty in flow in the river channel because of the intense exchange of sediment load on riverbeds and banks. Analysis of characteristics of confluent floods is able to improve our understanding of flood routing of backwater refluxing and sediment transportation in the middle Yellow River.

Acknowledgements

We acknowledge with gratitude the research grants kindly provided by the Hundred-talent Project of the Chinese Academy of Sciences (20110009), the Innovation Frontier Project of Institute of Soil and Water Conservation of the Chinese Academy of Sciences (10502), Key Research Program of the *Chinese Academy* of Sciences (Grant No. KZZD-EW-04), Strategic Priority Research Program of the Chinese Academy of Sciences (Grant No. XDB03020300), and State Key Laboratory of Soil Erosion and Dryland Farming on the Loess Plateau (10501-192, K318009902-1402).

References

Alpert, P., Krichak, S.O., Shafir, H., Haim, D., Osetinsky, I., 2008. Climatic trends to extremes employing regional modeling and statistical interpretation over the E. Mediterranean. Global and Planetary Change 63, 163–170.
ASCE Task Committee, 2000a. Artificial neural networks in hydrology. I: preliminary concepts. Journal of Hydraulic Engineering 5 (2), 115–123.
ASCE Task Committee, 2000b. Artificial neural networks in hydrology. II: hydrologic applications. Journal of Hydraulic Engineering 5 (2), 124–137.
Bartholy, J., Pongrácz, R., 2007. Regional analysis of extreme temperature and precipitation indices for the Carpathian Basin from 1946 to 2001. Global and Planetary Change 57, 83–95.
Begin, Z.B., 1986. Curvature ratio and rate of river bend migration update. Journal of Hydraulic Engineering 112 (10), 904–908.
Beven, K.J., 1997. TOPMODEL: a critique. Hydrological Processes 11, 1069–1086.
Bobee, B., Mathier, L., Perron, H., Trudel, P., Rasmussen, P.F., Cavadias, G., Bernier, J., Nguyen, V.T.V., Pandey, G., Ashkar, F., Ouarda, T.B.M.J., Adamowski, K., Alila, Y., Daviau, J.L., Gingras, D., Liang, G.C., Rousselle, J., Birikundavyi, S., RibeiroCorrea, J., Roy, R., Pilon, P.J., 1996. Presentation and review of some methods for regional flood frequency analysis. Journal of Hydrology 186, 63–84.
Burn, D.H., 1990. Evaluation of regional flood frequency analysis with a region of influence approach. Water Resources Research 26, 2257–2265.
Burn, D.H., 1997. Catchment similarity for regional flood frequency analysis using seasonality measures. Journal of Hydrology 202, 212–230.
Camacho, L.A., Lees, M.J., 1999. Multilinear discrete lag-cascade model for channel routing. Journal of Hydrology 226, 30–47.
Carrivick, J.L., 2006. Application of 2D hydrodynamic modelling to high-magnitude outburst floods: an example from Kverkfjoll, Iceland. Journal of Hydrology 321, 187–199.
Christensen, J.H., Christensen, O.B., 2003. Severe summertime flooding in Europe. Nature 421, 805–806.
Cunnane, C., 1988. Methods and merits of regional flood frequency analysis. Journal of Hydrology 100, 269–290.
Daluz, V.J.H., 1983. Conditions governing the use of approximations for the Saint-Venant equations for shallow surface water flow. Journal of Hydrology 60, 43–58.
Diodato, N., Bellocchi, G., 2012. Decadal modelling of rainfall-runoff erosivity in the Euro-Mediterranean region using extreme precipitation indices. Global and Planetary Change 86–87, 79–91.
Elleder, L., 2010. Reconstruction of the 1784 flood hydrograph for the Vltava River in Prague, Czech Republic. Global and Planetary Change 70, 117–124.
Glaser, R., Stangl, H., 2003. Historical floods in the Dutch Rhine Delta. Natural Hazards and Earth System Sciences 3, 1–9.
Greenbaum, N., Schwartz, U., Bergman, N., 2010. Extreme floods and short-term hydroclimatological fluctuations in the hyper-arid Dead Sea region, Israel. Global and Planetary Change 70, 125–137.
Haykin, S., 1999. Neural Networks: a Comprehensive Foundation, second ed. Prentice Hall, Upper Saddle River, New Jersey.
He, H.M., Yu, Q., Zhou, J., Tian, Y.Q., 2008. Modelling complex flood flow evolution in the Middle Yellow River China. Journal of Hydrology 353, 76–92.
He, H.M., Zhou, J., Yu, Q., Tian, Y.Q., Chen, R.F., 2006. Flood frequency and routing processes at a confluence of the middle Yellow River in China. River Research and Applications 22, 1–21.
Herget, J., Meurs, H., 2010. Reconstructing peak discharges for historic flood levels in the city of Cologne, Germany. Global and Planetary Change 70, 108–116.
Hisdal, H., Tveito, O.E., 1993. Extension of runoff series by the use of empirical orthogonal functions. Hydrology Science Journal 38, 33–50.
Huang, M.S., 1989. China History Floods (Upper Volume). Cathay Bookshop Publishing House, Beijing, pp. 120–135.
Jain, S., Lall, U., 2000. The magnitude and timing of annual maximum floods: trends and large-scale Climatic Associations for the Blacksmith Fork River, Utah. Water Resources Research 36 (12), 3641–3652.
Javelle, P., Ouarda, T.B.M.J., Lang, M., Bobee, B., Galea, G., Gresillon, J.M., 2002. Development of regional flood-duration-frequency curves based on the index-flood method. Journal of Hydrology 258, 249–259.
Jun-Haeng, H., Boes, D.C., Salas, J.D., 2001. Regional food frequency analysis based on a Weibull model: Part 1, Estimation and asymptotic variances. Journal of Hydrology 242, 157–170.
Kehew, A.E., Milewski, A., Soliman, F., 2010. Reconstructing an extreme flood from boulder transport and rainfall-runoff modelling: Wadi Isla, South Sinai, Egypt. Global and Planetary Change 70, 64–75.
Keskin, M.E., Agiralioglu, N., 1997. A simplified dynamic model for flood routing in rectangular channels. Journal of Hydrology 202, 302–314.
Loboda, N.S., Glushkov, A.V., Khokhlov, V.N., 2005. Using meteorological data for reconstruction of annual runoff series over an ungauged area: empirical orthogonal function approach to Moldova-Southwest Ukraine region. Atmospheric Research 77 (1–4), 100–113.
Macdonald, A.R., Werritty, B.A., 2001. Historical and Pooled Flood Frequency Analysis for River Ouse, York, UK. http://www.nwl.ac.cn/hec/seclected papers/floods.html.
McKillop, R.J., Clague, J.J., 2007. Statistical, remote sensing-based approach for estimating the probability of catastrophic drainage from moraine-dammed lakes in southwestern British Columbia. Global and Planetary Change 56, 153–171.

Mudelsee, M., Borngen, M., Tetzlaff, G., Grunewald, U., 2003. No upward trends in the occurrence of extreme floods in central Europe. Nature 425, 166–169.
Naidu, C.V., Satyanarayana, G.C., Durgalakshmi, K., Malleswara Rao, L., Jeevana Mounika, G., Raju, A.D., 2012. Changes in the frequencies of northeast monsoon rainy days in the global warming. Global and Planetary Change 92–93, 40–47.
Obled, Ch, Creutin, J.D., 1986. Some developments in the use of empirical orthogonal functions for mapping meteorological fields. Journal of Applied Meteorology 25, 1189–1204.
Palmer, T.N., Raisanen, J., 2002. Quantifying the risk of extreme seasonal rainfall events in a changing climate. Nature 415, 512–514.
Qian, L., 1992. Climate of the Loess Plateau, China. Meteorological Press, Beijing, pp. 213–256.
Ramamurthy, A.S., 1990. Dividing flow in open channels. Journal of Hydraulic Engineering 116, 449–455.
Rao, A., Hsieh, C.H., 1991. Estimation of variables at ungauged locations by Empirical Orthogonal Functions. Journal of Hydrology 123, 51–67.
Ren, X., Cheng, J., 2003. River Hydrology. Hohai University Press, Nanjing, pp. 110–143.
Sudheer, K.P., Gosain, A.K., Ramasastri, K.S., 2002. A data driven algorithm for constructing artificial neural network rainfall-runoff models. Hydrological Process 16 (6), 1325–1330.
Tramblay, Y., Badi, W., Driouech, F., El Adlouni, S., Neppel, L., Servat, E., 2012. Climate change impacts on extreme precipitation in Morocco. Global and Planetary Change 82–83, 104–114.
Walters, R.A., Cheng, R.T., 1980. Accuracy of an Estuarine hydrodynamic model using smooth elements. Water Resources Research 16, 187–195.
Wang, X., 2004. The research on the flood peak flow forecast of Jiaokou in flood season. Journal of Northwest Hydroelectric 20 (3), 62–64.
Yu, S., Lin, X., 1996. Abrupt change of drought/flood for the Last 522 years in the middle reaches of yellow. Quarterly Journal of Applied Meteorology 7 (1), 89–95.
Zolina, O., Kapala, A., Simmer, C., Gulev, S.K., 2004. Analysis of extreme precipitation over Europe from different reanalyses: a comparative assessment. Global and Planetary Change 44, 129–161.